



Characterization and Delineation of Potential Evaporite Geohazards Using Electrical Resistivity Methods along FM 2185, Culberson County, Texas

Lenora D. Perkins, Kevin W. Stafford, and Wesley A. Brown

Department of Geology, Stephen F. Austin State University, Box 13011, Nacogdoches, Texas 75962, U.S.A.

ABSTRACT

Extensive karst development within the Delaware Basin of West Texas and southeastern New Mexico poses a significant threat to infrastructure. Dissolution of regional evaporite strata have led to karst geohazards including sinkholes, subsidence features, and caves. The study area is located within the Gypsum Plain in Culberson County, Texas, and includes outcrops of Permian Castile and Rustler strata that host gypsum karst. Land reconnaissance surveys conducted during summer of 2019 documented numerous surface karst features proximal to Farm to Market Road 2185 (FM 2185). In combination with traditional survey techniques, electrical resistivity methods were used to delineate karst features along a 48 km segment of FM 2185.

Capacitively-coupled resistivity (CCR) and direct-current resistivity (DCR) methods were used to characterize evaporite karst features that do not manifest surficially but pose potential geohazard concerns. CCR data were acquired using the Geometrics OhmMapper G-858 resistivity system, which uses a dipole-dipole configuration composed of five receivers connected by 2.5 m coaxial cables and a transmitter offset of 2.5 m. In combination with the medium analyzed, this geometric configuration enabled resistivity soundings up to 2.5 m deep. DCR data was collected with a SuperSting (R8/IP) multi-electrode earth resistivity meter using 112 electrodes with 2 m spacing and a dipole-dipole array configuration. This enabled a depth of investigation of up to 25 m. Data were processed using Advanced Geosciences Inc.'s (AGI's) EarthImager 2D software and used to delineate and characterize karst-related geohazards in the shallow subsurface within the study area. Five sites are presented to demonstrate karst variability and electrical resistivity method effectiveness in geohazard detection in gypsum strata.

INTRODUCTION

The Delaware Basin of West Texas and southeast New Mexico hosts widespread karst development throughout the Gypsum Plain, which covers an area of ~2800 km² (Hill, 1996). The evaporite outcrops found within this area include Permian-aged Castile Formation and lower Rustler strata. Features commonly expressed in this region are comprised of a wide array of surficial karst, as well as shallow epigene caves, and deeper, more complex hypogene cave systems (Stafford et al., 2008a, 2008b). Evaporite karst systems can be complex and rapidly evolve due to higher solution rates than carbonates. Depending on hydrogeologic conditions, dissolution of evaporite karst can occur within days, weeks, or years while in carbonate karst, the rates of void enlargement rarely achieve significance within the human lifetime (Klimchouk and Aksem, 2005).

Oil exploration in the Permian Basin has a long and rich history since the 1920s. As of January 2020, the Permian Basin has produced more than 35.6 billion barrels of oil and ~125 trillion cubic ft of natural gas (EIA, 2020). Within the last decade there have been advances in the Delaware Basin targeting unconventional reservoirs such as the Bone Spring Formation and the Delaware Mountain Group (EIA, 2020). The intensification in hydrocarbon extraction and exploration has led to an increase in development of transportation infrastructure along with an associated rise of incidents related to karst geohazards. According to Stafford et al. (2017), the existing roads in this area were not initially designed to accommodate the heavy volume, and weight, of oilfield traffic and therefore are more prone to collapse.

Traditional survey techniques such as field mapping may be used to identify karst hazards that occur at the land surface in areas with absent or patchy cover sediments (Neukum et al., 2010). However, karst features that do not manifest surficially require alternative surveying methods to characterize the extent of subsurface features at depth. Over the past decade, various methods have been implemented to characterize occurrence of Gypsum Plain karst, and due to the expansion of oilfield activity into the region; remote sensing; and GIS (geographic information system) techniques have been used more frequently (Stafford et al., 2008b, 2017; Woodard, 2017; Majzoub et al., 2017; Land et

al., 2018). Studies conducted by [Majzoub et al. \(2017\)](#) and [Land et al. \(2018\)](#) demonstrated the effectiveness of direct-current resistivity (DCR) tomography in the detection of karst geohazards, and [Woodard \(2017\)](#) and [Stafford et al. \(2017\)](#) demonstrated that capacitively-coupled resistivity (CCR) surveys are equally as effective.

This study was conducted along a 48 km segment of undeveloped Farm to Market Road 2185 (FM 2185) in Culberson County, Texas ([Fig. 1](#)). The dissolution of evaporite strata of the Castile and Rustler formations have led to the formation of numerous karst geohazards including sinkholes, subsidence features, and caves. Land reconnaissance surveys conducted during summer of 2019 documented numerous surface karst features along FM 2185. This study effectively combines both CCR and DCR methods to delineate and characterize concealed karst features that could lead to potential geohazard concerns. Five survey sites are presented in this study as examples of the effectiveness of the CCR imaging in the rapid delineation of potential geohazards. Of the five sites studied, two were selected for comparative DCR survey analyses based on observable karst processes and potential subsurface karst geohazards characterized by CCR data.

Geologic Setting

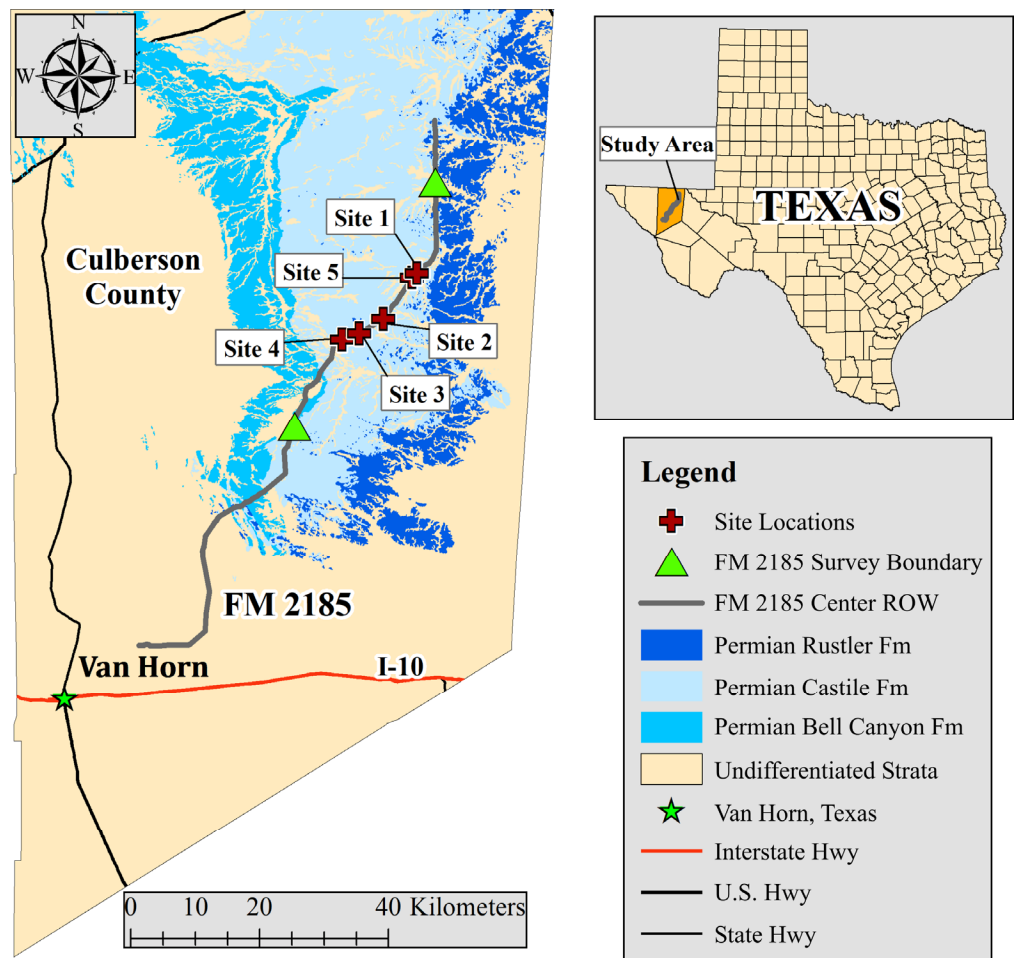
The Delaware Basin of West Texas and southeastern New Mexico is an irregular, inverted pear-shaped intracratonic depositional basin ([Fig. 2](#)). As the major western subdivision of the Permian Basin, it encompasses an area of 33,500 km² with a length of 250 km and width of 180 km that is restricted by the

Capitan Reef Complex ([Hill, 1996](#)). From the late Precambrian to the Late Mississippian, the Delaware Basin was part of the Tobosa Basin. During that time, shelf sediments accumulated in a “layer-cake” fashion due to passive subsidence, as well as the warping and sagging of the Tobosa Basin ([Horak, 1985](#)).

During the Late Mississippian through Early Permian (310–265 Ma), a major tectonic episode occurred in the area of the Delaware Basin. Initiated by the formation of Pangea, mild tectonic activity accompanied vertical movement along zones of weakness from late Precambrian lateral faulting ([Keller et al., 1980](#)). This tectonic episode produced the Ouachita Orogeny in the Marathon-Delaware Basin area. Additionally, uplift of the Central Basin Platform induced the division of the Tobosa Basin into three segments: the uplifted Central Basin Platform, and the down-dropped Delaware and Midland basins ([Hill, 1996](#)). Broad limestone shelves grew to surround the smaller basins as they formed. Stream channels eventually cut through the limestone shelves to deposit fine sands and shales into the basins ([Keller et al., 1980](#)). In the Pennsylvanian, increased compression from the Ouachita orogenic front led to the rapid subsidence of the Delaware Basin, where it remained a deep-water basin until the end of the Guadalupian time ([Hill, 1996](#)).

Extensive reef growth occurred during the Ochoan, which restricted the flow of open marine waters and encouraged the formation of a deep saline lake that possessed conditions conducive for the deposition of Castile evaporites. Although the Castile deposition was limited to the Delaware Basin, the deposition of Salado and Rustler strata capped the region and surrounding basins ([Scholle et al., 2004](#)). The tectonic activity that occurred

Figure 1. Location of the study area; FM 2185 in thickened gray line stretching southwest to northeast across Culberson County, Texas. Survey sites are indicated by red crosses with survey boundary indicated by green triangles.



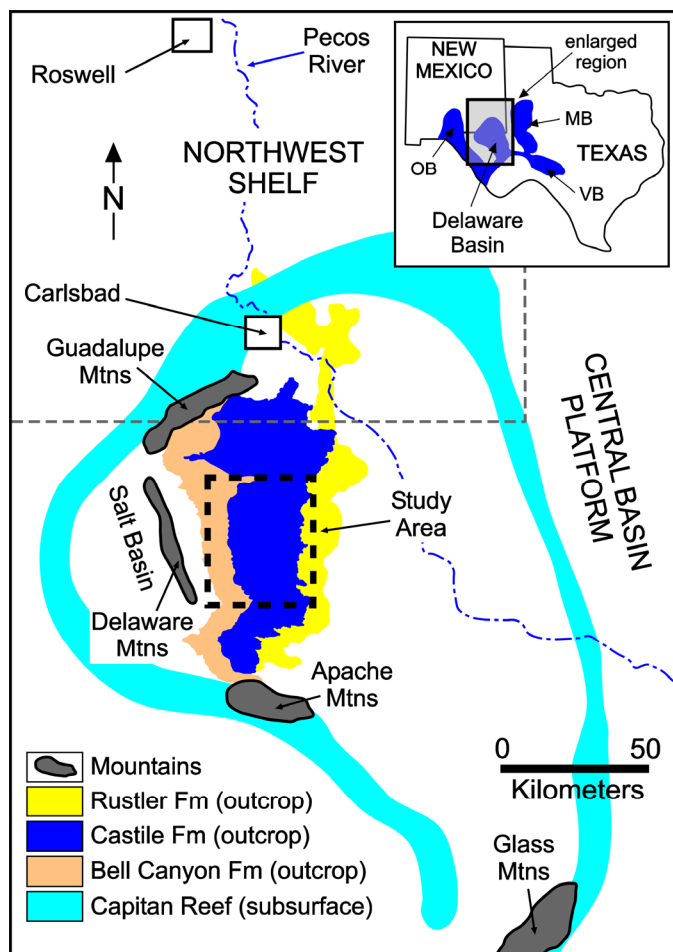


Figure 2. Map illustrating the location of the Delaware Basin in West Texas and southeastern New Mexico, including the primary geologic features of the region. The study area is outlined by the dashed black line. MB = Midland Basin.

during the Early Mesozoic had little effect on the Delaware Basin; however, the Laramide Orogeny of the Late Mesozoic and Early Cenozoic produced regional tilting and uplift of the basin strata 3–5° to the east-northeast (Decker et al., 2018).

Following Laramide deformation, the Basin and Range phase consisted of lithospheric thinning, extension, and normal faulting. Volcanism also ensued during this time to produce a regime of higher heat flow in the Delaware Basin with geothermal gradients reaching 40–50° C/km or more (Barker and Pawliewicz, 1987). The hydrothermal regime shifted from one of melting and igneous intrusions to one of an increased temperature gradient and convective heat flow. During the Oligocene, hydrothermal cells were formed by igneous intrusions which allowed deeply circulating fluids to move along fault zones and paleokarst systems (Decker et al., 2018).

During the Quaternary, both the effects of Basin and Range extension and the geothermal gradient decreased. The present-day geothermal gradient in the Delaware Basin is roughly 20°C/km as compared to the Miocene paleogradient of 40–50°C/km (Barker and Halley, 1986; Barker and Pawliewicz, 1993). Additionally, during the Pleistocene, the Delaware Basin experienced considerable fluctuations in climate from wet and cold to dry and warm during glacial and interglacial periods. The modern landscape of the Gypsum Plain was sculpted through intermittent periods of heavy stream erosion during glacial melt and karst processes. Over the last 10,000 yr, the changes in climate al-

lowed the Delaware Basin to transition from a cool and wet climate to one that is dry and arid-semiarid.

Karst Development

The Permian evaporites of the Gypsum Plain have resulted in a quickly evolving landscape throughout the Delaware Basin. The Castile Formation is the largest continuous outcrop of evaporites in the area and represent deep-water deposits, which were subsequently covered by the Salado and Rustler formations. Minor occurrences of karst development are noted in the evaporites of lower Rustler strata located on the eastern portion of the study area. The halite-rich Salado Formation is almost completely dissolved from outcrop and shallow subcrop via intrastatal dissolution, thus forming an irregular solutional contact boundary between the Castile and Rustler strata (Stafford et al., 2008a). The lower bounding horizon is the siliciclastic Bell Canyon Formation, which provides ascending fluids for hypogene speleogenesis (Stafford et al., 2018). Models of the current and paleo hydrogeologic system of the Delaware Basin, derived by Lee and Williams (2000), indicate that the Bell Canyon aquifer is mixing ascending fluids and hydrocarbons from deep basinal units.

In the Delaware Basin, the Castile Formation hosts extensive cave and karst development across 1800 km² of outcrop. Surficial karren dominate the landscape with abundant sinkholes, subsidence features, and solution-widened fractures. Epigene and hypogene speleogenesis both account for the formation of solutional caves in this region. Epigene caves develop from gravitationally driven water from near-surface meteoric processes in unconfined strata, while hypogene caves manifest via dissolution from rising fluids from the underlying Bell Canyon Formation, driven by differences in hydraulic pressure gradients through semi-confined strata (Stafford et al., 2008a).

Also present within the study area are gypsite suffosion caves, or gypsite soil caves, and collapsed breccia pipes. Suffosion caves commonly develop from the preferential transport of gypsic soils through thick soil horizons and soil-filled solutional sinkholes (Stafford et al., 2017). Zones of brecciation, which extend laterally and vertically hundreds of meters, formed as the result of intrastatal dissolution of evaporites at depth through hypogene speleogenesis (Stafford et al., 2008a).

ELECTRICAL RESISTIVITY METHODS

A continuous CCR survey was conducted along a 48 km segment of the proposed route of FM 2185 in Culberson County, Texas (Fig. 1). The CCR data was acquired with the Geometrics OhmMapper G–858 resistivity system with a dipole-dipole TR-5 configuration composed of five receivers and one transmitter connected by 2.5 m coaxial cables, and a transmitter offset of 2.5 m. The OhmMapper G–858 resistivity meter was attached to a vehicle and towed at ~2.5–3 km/hr). Data were collected at a transmission rate of once per second. A Trimble Nomad 900 series logger, a global positioning system (GPS) unit, connected to a Pathfinder Pro receiver and Zephyr antennae recorded the traverse of the survey with a horizontal accuracy of less than 50 cm.

Five sites of interest, each 120 m long, were selected based on observable surficial karst geohazards near the proposed right of way (ROW) of FM 2185. Two-dimensional DCR surveys were conducted at two of the five sites of interest, sites 4 and 5, using methods adapted from Majzoub et al. (2017), which utilized an eight-channel SuperSting (R8/IP) multi-electrode earth resistivity meter produced by Advanced Geosciences Inc. (AGI, 2007). DCR surveys were conducted at 2 m electrode spacing using 112 electrodes arranged in a dipole-dipole configuration. The total DCR survey length for sites 4 and 5 were 222 m each.

Prior to inversion, the quality of the CCR data and GPS points gathered with the OhmMapper G–858 resistivity meter

were preprocessed using MagMap2000, a pre-inversion software program developed by Geometrics. AGI's EarthImager 2D inverse modelling software was used to invert collected resistivity data. To accurately represent the elevation variance at each site, terrain corrections were applied. Elevation values were extracted from a digital elevation model created from lidar (light detection and ranging) data of the study area and processed in ArcGIS. Lidar horizontal resolution was acquired at 0.3–0.4 m with 10 cm vertical resolution provided by the Texas Department of Transportation (TxDOT) (Ehrhart, 2016).

RESULTS AND INTERPRETATIONS

Site 1 (120 m Survey)

The survey of site 1 was conducted in a SW–NE trending line within the Castile Formation. The region is noted by a gradual elevation difference of 3 m, sloping downward to the northeast. Data presented is a 120 m segment of CCR data extracted from ~1 km of continuous CCR survey of an undeveloped segment of FM 2185 (Figs. 3A–1 and 3A–2). Effective depth of investigation is ~2.5 m. Site 1 is included as a control site since there are no significant karst hazards revealed along this section of study. A thin layer of gypsic soil (gypsite) is present to 0.5–1.0 m depth throughout the resistivity inversion. This overlies gypsum bedrock with slightly variable moisture content likely indicative of minor regions of enhanced porosity within Castile gypsum.

Site 2 (120 m Survey)

Site 2, located within the Castile Formation, contains numerous sub-vertical, solution-widened fractures in gypsite creating preferential pathways to the underlying irregular gypsum bedrock surface (Figs. 3B–1 and 3B–2). The region is noted by an elevation difference of 2.8 m and sparse vegetation. Data presented is a 120 m segment of CCR data extracted from ~1 km of continuous CCR survey of an undeveloped segment of FM 2185. Effective depth of investigation is ~2.5 m.

This site is proximal to a mapped surficial karst feature, a near vertical solution conduit through gypsite with smooth cusped walls, and numerous anomalous patterns were modeled within the resistivity inversions. Vertical fractures associated with gypsite are interpreted through the resistivity profile beginning at meter mark 5 and extending through the 110 m mark. From meter mark 65 to 100 is an area of higher resistivity signatures in relation to high density vertical fractures in gypsite. Low resistivity signatures in relation to gypsum bedrock are seen through the entire resistivity section.

Site 3 (120 m Survey)

Site 3, located within the Castile Formation, contains shallow gypsic soil, 0.5–1.0 m depth, overlying a non-uniformly cemented breccia pipe that has been largely calcitized through sulfate reduction associated with hypogene processes (Stafford et al., 2008c). The land surface exhibits an elevation difference of 1 m, moderate vegetation, and proximal surface exposures of indurated gypsic soil, poorly-cemented brecciated gypsum, and cemented calcitized breccia. Data presented is a 120 m segment of CCR data extracted from ~1 km of continuous CCR survey of an undeveloped segment of FM 2185. Successful depth of investigation is ~2.5 m.

The resistivity image presented in Figures 4C–1 and 4C–2 displays a portion of the breccia pipe that extends from meter mark 0 to 95 and 105 to 115 along the resistivity profile, which is likely connected at depths greater than CCR investigation. High resistivity signature within the breccia pipe at meter mark 47 is interpreted as probable fracturing and high moisture flux. Within the breccia pipe, well-cemented brecciated gypsum and porous,

poorly-cemented, calcitized areas are discernable, likely a result of fluctuating moisture content within variably porous media.

Site 4 (120 m Survey)

Site 4, located in a broad collapse area within the Castile Formation, is significantly infilled with gypsic soil. The region is noted by an elevation difference of 0.9 m, a change in soil color/composition in relation to the surrounding area, and dense vegetation. Data presented are a 120 m segment of CCR data extracted from ~1 km of continuous CCR survey of an undeveloped segment of FM 2185, and a 120 m segment of a DCR survey conducted with 112 electrodes at 2.0 m spacing (Fig. 4). Successful depth of investigation is to 2.5 m and 25 m for the CCR and DCR data, respectively.

This site is proximal to dense vegetation and mapped surficial karst features. Multiple anomalous patterns were modeled within resistivity inversions. Observed in the inverted CCR data (Figs. 4A–1 and 4A–2) from meter mark 0–5, and 0.5–1.0 m in depth, is a zone of fractured gypsite overlying a low resistivity anomaly associated with moisture-rich gypsic soils at 1–2.5 m depth. At meter mark 10 to 15, and 1–2.5 m deep, a high resistivity anomaly is interpreted as a probable suffosion cave surrounded by a moisture gradient, probably associated with the low resistivity anomaly of moisture-rich gypsic soils. From meter mark 15 to 70 is an area of higher resistivity signatures in relation to collapsed gypsite exposed in the road surface. Low resistivity signatures in relation to a collapsed sink retaining higher moisture are seen from meter mark 75 to 105. This interpretation is supported by orthoimagery (Fig. 4C–1) and the elevation model derived from lidar (Fig. 4C–2). The presence of abundant vegetation indicates areas of elevated moisture content locally. The elevation model derived from lidar correlates internal sinkholes located within a larger depression. A second probable suffosion cave is noted by higher resistivity signatures at meter mark 115–120 at depth of 1–2.5 m.

The DCR data reflects the gypsite/gypsum bedrock boundary at ~1.5 m in depth (Figs. 4B–1 and 4B–2). Shallow, high resistivity anomalies observed within the gypsite are interpreted as probable suffosion caves, which correlates well with CCR analyses. The low resistivity anomaly at meter mark 20 is associated with dense vegetation and elevated moisture overlying a collapsed brecciated region, ~3–12 m deep. From meter mark 75 to 115 is a region of low resistivity is association with the surficial recharge area of a collapsed brecciated region. At greater depths, within gypsic bedrock from meter mark ~30 to 115, is a low resistivity region of un-cemented breccia with subsequent collapse. The higher resistivity anomaly observed at meter mark 25 to 40 is a probable suffosion cave associated with drier conditions within the proximal gypsum.

Site 5 (120 m Survey)

Site 5 is located in an area of the Castile Formation significantly mantled and infilled with gypsic soil. The region is noted by an elevation difference of 0.5 m and an area of dense vegetation. Data presented are a 120 m segment of CCR data extracted from ~1 km of continuous CCR survey of an undeveloped segment of FM 2185, and a 120 m segment of a DC resistivity survey conducted with 112 electrodes at 2.0 m spacing (Fig. 5). Successful depth of investigation is to 2.5 m and 25 m for the CC and DC resistivity data, respectively.

This site is proximal to mapped surficial karst features (Figs. 5C–1 and 5C–2) and numerous anomalous patterns were modeled within the resistivity inversions. Within the CCR data (Figs. 5A–1 and 5A–2), from meter mark 5 to 45, and 0.5–2.5 m in depth, is a zone of extensively collapsed gypsite. At meter mark 35 and 65, and 2.0 m deep, a high resistivity anomaly is interpreted as a probable, un-collapsed gypsite cave. In DCR data

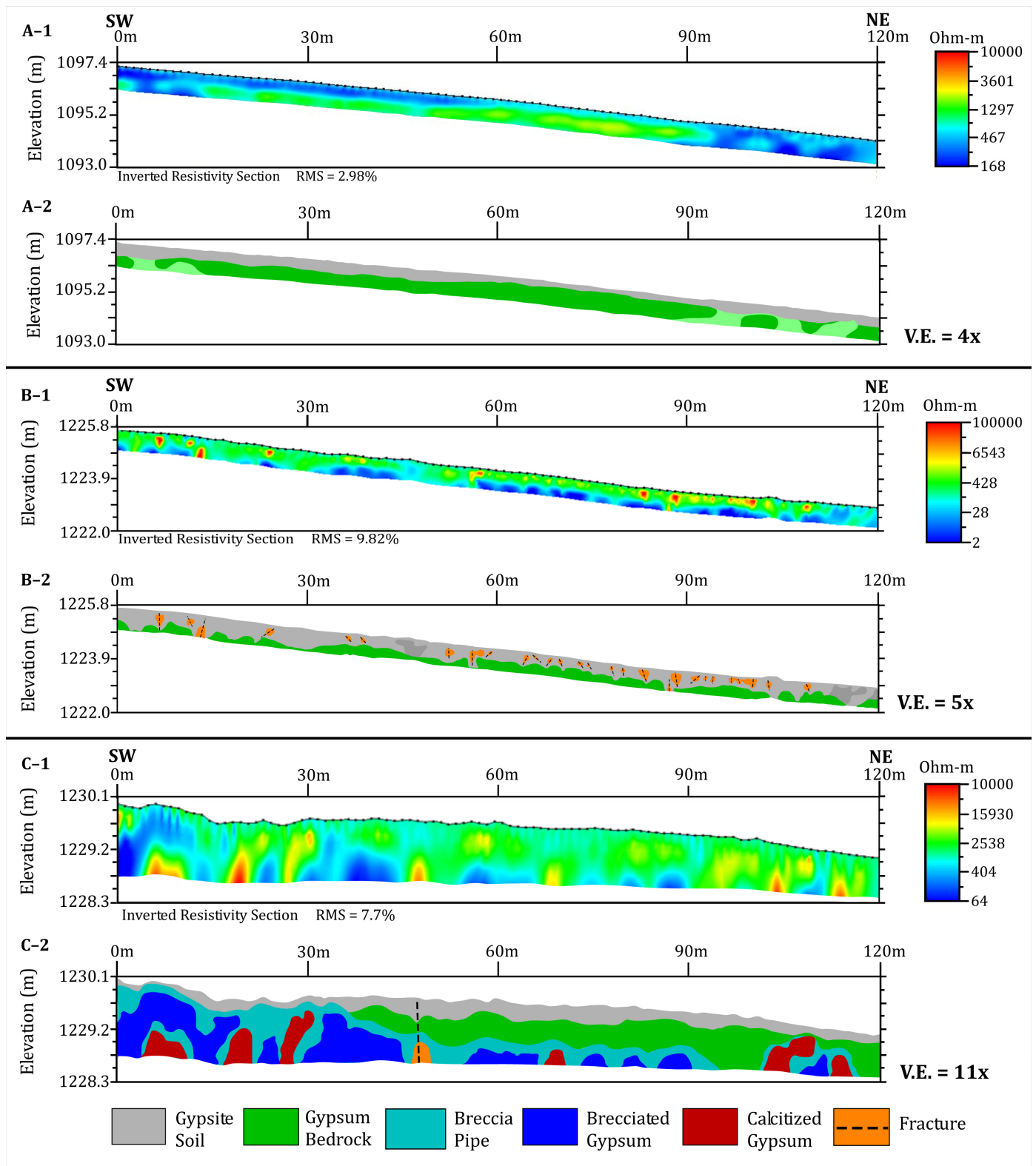


Figure 3. (A-1) Site 1, 120 m segment of CCR data inverted resistivity section, RMS = 2.98%, and (A-2) site 1 interpreted inverted section. Depth of investigation is ~2.5 m; vertical exaggeration of 4x. (B-1) Site 2, 120 m segment of CCR data inverted resistivity section, RMS = 9.82%, and (B-2) site 2 interpreted inverted section. Depth of investigation is ~2.5 m; vertical exaggeration of 5x. (C-1) Site 3, 120 m segment of CCR data inverted resistivity section, RMS = 7.7%, and (C-2) site 3 interpreted inverted section. Depth of investigation is ~2.5 m; vertical exaggeration of 11x.

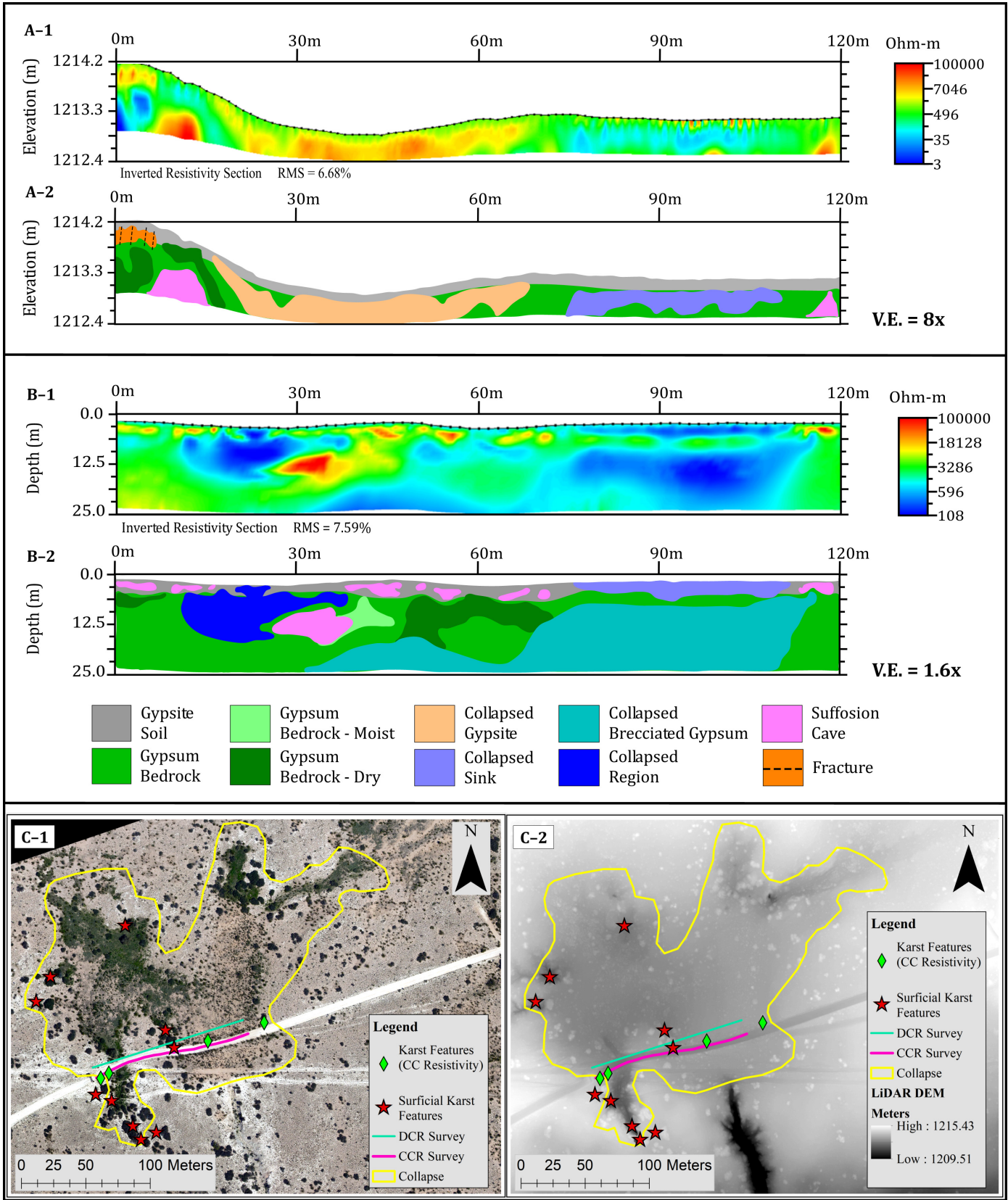


Figure 4. Site 4, 120 m segment of CCR and DCR data. (A-1) CCR inverted resistivity section to depth of ~2.5 m, RMS = 6.68%, and (A-2) CCR interpreted inverted section. (B-1) DCR inverted resistivity section to depth of ~25 m, RMS = 7.59%, and (B-2) DCR interpreted inverted section. Note vertical exaggeration of 8x and 1.6x for CCR and DCR, respectively. (C-1) Orthoimagery of the region of collapse and (C-2) elevation model derived from lidar of the region of collapse. Green diamonds represent potential karst features traversed by CCR survey and interpreted in A-2; red stars indicate mapped surficial karst features.

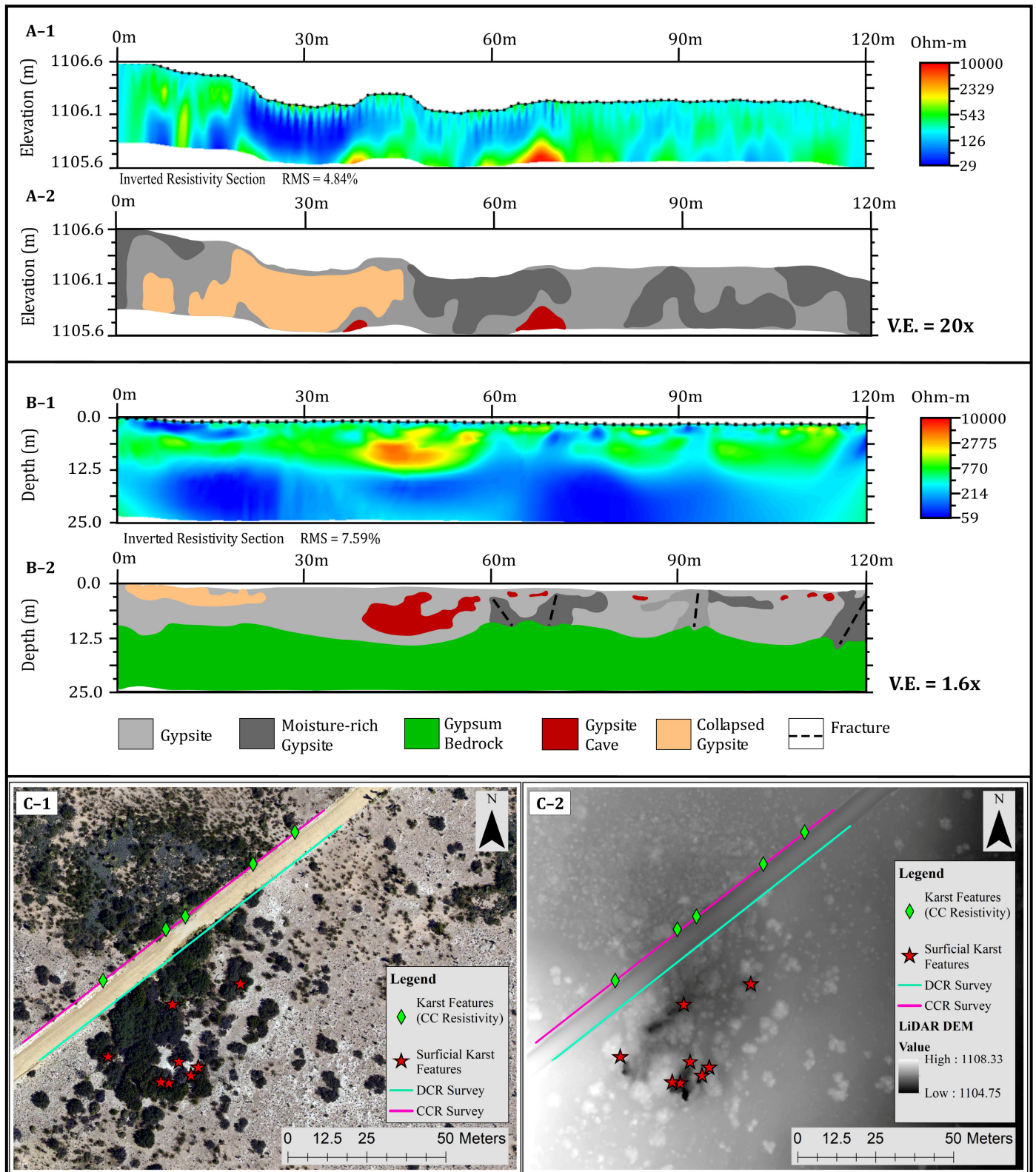


Figure 5. Site 5, 120 m segment of CCR and DCR data. (A-1) CCR inverted resistivity section to depth of ~2.5 m, RMS = 4.84%, and (A-2) CCR interpreted inverted section. (B-1) DCR inverted resistivity section to depth of ~25 m, RMS = 3.48%, and (B-2) DCR interpreted inverted section. Note vertical exaggeration of 20x and 1.6x for CCR and DCR, respectively. (C-1) Orthoimagery of site 5 and (C-2) elevation model derived from lidar. Green diamonds represent potential karst features traversed by CCR survey and interpreted in A-2; red stars indicate mapped surficial karst features, pink line is CCR survey line, and teal line is DCR survey line.

(Figs. 5B–1 and 5B–2), from meter mark 3 to 20, and 2.5 m deep, is a zone of collapsed gypsite. At meter mark 40 to 58, and depth of 2.5–3.5 m, a high resistivity anomaly is interpreted as a probable gypsite cave. Similar features are noted at shallower depths between meter mark 60 to 120. Areas of low resistivity at meter mark 60 to 75, 85 to 105, and 115 to 120 and to 5 m in depth are interpreted as areas of fractured, moisture-rich gypsite. The gypsite/gypsum bedrock interface is interpreted to be at ~5 m in depth.

DISCUSSION

Karst Phenomena

The Gypsum Plain of the Delaware Basin encompasses outcrop of strata that are dominantly composed of gypsum or anhydrite of the Castile Formation (Olive, 1957). Karst development is the result of a complex interaction between surficial geomorphology, hydrogeologic regimes on a local and regional scale, and local variations in lithology (Stafford et al., 2008a). Evaporitic rocks possess high solubility and have the potential to form dramatic karst landscapes through natural processes and intensified by anthropogenic modifications. Within the study area, suffosion karst have the highest geohazard potential and are likely connected to deeper karst features that allow sediment and fluid transport. Due to the low permeability of gypsum, heavy rain events dissolve the evaporite rocks primarily by widening solution fractures within gypsum bedrock. The solution fractures enable fluids to migrate through sulfate rocks promoting development of conduits and enabling greater piping rates of gypsite soil, that subsequently collapse. This study illustrates a range of geohazards from areas of fractured bedrock (site 2), brecciation and calcitization (site 3), to more significant hazards such as caves (sites 4 and 5).

Site 1, acting as a control site with no karst geohazards detected, has a thin layer of gypsite soil overlaying solid gypsum bedrock with small areas of moisture present. At site 2, the soil-bedrock interface becomes more irregular with the presence of vertical fractures through gypsite and minor karsting along the soil/bedrock contact. The survey of site 2 was conducted in an area of sparse vegetation, which positively correlates with the anomalous patterns modeled within the resistivity inversions. The vegetation exploits higher soil water retention, with preferential root growth along fracture planes.

Throughout the Gypsum Plain, zones of brecciation have been well-documented in the evaporite strata of the Castile, Salado, and Rustler formations (Anderson and Kirkland, 1980). Breccia forms from intrastatal dissolution of evaporites through hypogene speleogenesis where ascending fluids create void space that later collapsed. Calcitization is commonly found in regions of brecciation forming vertically and laterally extensive calcitized breccia zones. The same transmissive and soluble zones that allow for hypogene dissolution and brecciation create preferential flow paths for ascending hydrocarbons, which serve as the energy source for sulfate reducing bacteria associated with evaporite calcitization (Hill, 1996). Study site 3 contains signature anomalies of a breccia pipe containing both brecciated gypsum and “plume-like” structures of calcitized gypsum associated with ascending light hydrocarbons.

The inverted resistivity sections observed from the CCR surveys collected at site 4 and site 5 (Figs. 4 and 5) revealed the presence of significant karst geohazards. Combined with the close proximity and dense clustering of surficially mapped karst features, DCR methods were employed to obtain greater depth of investigation. The karst development at site 4 (Fig. 4) appears to be a mixture of hypogene processes (i.e. collapsed brecciated gypsum), and epigene processes (i.e., numerous suffosion caves observed at the gypsite soil–bedrock boundary). Site 5 (Fig. 5) shows a much thicker gypsite soil horizon in the resistivity pro-

file section with a distinct contact with gypsum bedrock. Suffosion processes are interpreted to be the cause of both the observed fractures and the gypsite cave where soil has likely piped into the open gypsum cavities at depth.

Remote sensing data (orthoimagery and lidar data) provided by the TxDOT and surficial geohazard mapping conducted in the summer of 2019 assisted with the interpretations. The range of resistivity anomalies observed in the selected study sites correlated well with surface manifestations of karst geohazards, but also include features that are not observed at the land surface.

CONCLUSIONS

The numerous manifestations of evaporite karst found within the Gypsum Plain can be identified in resistivity imaging, as well as observed at the land surface throughout the outcrop region of the Castile Formation. The intensification in hydrocarbon extraction and exploration has led to an increase in development of transportation infrastructure along with an associated rise of incidents related to karst geohazards. A critical element for improved infrastructure design and geohazard mitigation is high-resolution characterization of potential geohazards that do not manifest at the land surface.

Previous studies conducted in the area have illustrated the independent effectiveness of CCR and DCR surveys, (Woodard, 2017; Majzoub et al., 2017; Stafford et al., 2017, 2018; Land et al., 2018). While CCR methods allow for the rapid delineation of shallow subsurface geohazards, it is limited in depth of investigation; DCR methods allow for high resolution and deeper investigations yet are time intensive. The combined application of CCR and DCR analyses utilizes the best aspects of each technique to characterize potential karst geohazards.

The study presented in this paper focused on a 48 km segment of undeveloped FM 2185 that traverses northward across the Gypsum Plain in Culberson County, Texas. Prior land reconnaissance surveys conducted during the summer of 2019 documented numerous surficial karst manifestations, including sinkholes, subsidence features, caves and lithologic variability. The full length of the study area (48 km) was initially surveyed utilizing CCR methods to rapidly delineate karst features, which do not currently manifest at the land surface, to depths up to ~2.5 m. In areas of high karst geohazard concern identified in CCR analyses that do not currently exhibit strong surface manifestations, DCR analyses enabled higher resolution characterization of potential geohazards both laterally and to a greater depth (~25 m).

The combination of non-invasive geophysical methods employed in this study quickly detected potential karst geohazards, but for proper characterization a combination of field mapping and excavation is required. The use of this technique, utilizing rapid CCR survey with the high resolution and greater depth of investigation of a DCR survey, can prove essential for geohazard mitigation and the improvement of vehicle infrastructure design to properly handle the weight and volume of oilfield traffic.

ACKNOWLEDGMENTS

This research was partially funded by the Texas Department of Transportation (TxDOT) with support from Stephen F. Austin State University Department of Geology and the Office of Research and Graduate Studies, as well as the West Texas Geological Society. The authors are grateful for the generous field assistance of the individuals that made this work possible: Melanie Ertons, Evan Bass, Andrew Brillon, and Joseph Amell. The comments of the reviewers are greatly appreciated in the improvement of this manuscript during the revision process.

REFERENCES CITED

AGI, 2007, Instruction manual for EarthImager 2D resistivity and IP inversion software: Advanced Geosciences, Inc., 139 p.

- Anderson, R. Y., and D. W. Kirkland, 1980, Dissolution of salt deposits by brine density flow: *Geology*, v. 8, p. 66–69.
- Barker, C. E., and R. B. Halley, 1986, Fluid inclusion, stable isotope, and vitrinite reflectance evidence for the thermal history of the Bone Spring Limestone, southern Guadalupe Mountains, Texas, *in* D. L. Gautier, ed., Roles of organic matter in sediment diagenesis: Society of Economic Paleontologists and Mineralogists Special Publication 38, p. 189–203.
- Barker, C. E., and M. J. Pawliewicz, 1987, The effects of igneous intrusions and higher heat flow on thermal maturity of Leonardian and younger rocks, western Delaware Basin, Texas, *in* D. W. Cromwell and L. Mazzullo, eds., Glass Mountains: Society of Economic Paleontologists and Mineralogists Guidebook, p. 69–83.
- Barker, C. E., and M. J. Pawliewicz, 1993, Post-tectonic reheating of portions of the Permian Basin as expressed by iso-reflectance lines on regional structural sections, *in* D. W. Love et al., eds., Carlsbad region, New Mexico and West Texas: New Mexico Geological Society 44th Annual Field Conference Guidebook, p. 29–30.
- Decker, D. D., V. J. Polyak, Y. Asmerom, and M. S. Lachniet, 2018, U–Pb dating of cave spar: A new shallow crust landscape evolution tool: *Tectonics*, v. 37, p. 208–223.
- Ehrhart, J. T., 2016, Speleogenesis and delineation of megaporosity and karst geohazards through geologic cave mapping and lidar analyses associated with infrastructure in Culberson County, Texas: M.S. Thesis, Stephen F. Austin State University, 66 p.
- EIA, 2020, Permian Basin, part 1: Wolfcamp, Bone Spring, Delaware shale plays of the Delaware Basin: U.S. Department of Energy Energy Information Association, 40 p.
- Hill, C. A., 1996, Geology of the Delaware Basin, Guadalupe, Apache and Glass mountains: New Mexico and West Texas: Permian Basin Section of the Society of Economic Paleontologists and Mineralogists Publication 96–39, 480 p.
- Horak, R. L., 1985, Trans-Pecos tectonism and its effects on the Permian Basin, *in* P. W. Dickerson and W. R. Muehlberger, eds., Structure and tectonics of Trans-Pecos, Texas: West Texas Geological Society Publication 85–81, p. 81–87.
- Keller, G. R., J. M. Hills, and R. Djeddi, 1980, A regional geological and geophysical study of the Delaware Basin, New Mexico and West Texas, *in* P. W. Dickerson and J. M. Hoffer, eds., Trans-Pecos region: New Mexico Geological Society 31st Annual Field Conference Guidebookp. 105–111.
- Klimchouk, A. B., and S. D. Aksem, 2005, Hydrochemistry and solution rates in gypsum karst: Case study from the Western Ukraine: *Environmental Geology*, v. 48, p. 307–319.
- Land, L., C. Cikoski, D. McCraw, and G. Veni, 2018, Karst geohazards and geophysical surveys: US 285, Eddy County, New Mexico: National Cave and Karst Research Institute Report of Investigation 7, 89 p.
- Lee, M. K., and D. D. Williams, 2000, Paleohydrology of the Delaware Basin, western Texas: overpressure development, hydrocarbon migration, and ore genesis: *American Association of Petroleum Geologists Bulletin*, v. 84, p. 961–974.
- Majzoub, A. F., K. W. Stafford, W. A. Brown, and J. T. Ehrhart, 2017, Characterization and delineation of gypsum karst geohazards using 2D electrical resistivity tomography in Culberson County, Texas, USA: *Journal of Environmental and Engineering Geophysics*, v. 22, p.411–420.
- Neukum, C., C. Grutzner, R. Azzam, and K. Reicherter, 2010, Mapping buried karst features with capacitive-coupled resistivity system (CCR) and ground penetrating radar (GPR), *in* B. Andreo, F. Carrasco, J. J. Duran, and J. W. LaMoreaux, eds., Advances in research in karst dedia: Springer, p. 429–434.
- Olive, W. W., 1957, Solution-subsidence troughs, Castile Formation of Gypsum Plain, Texas and New Mexico: *Geological Society of American Bulletin*, v. 68, p. 351–358.
- Scholle, P. A., R. H. Goldstein, and D. S. Ulmer-Scholle, 2004, Classic Upper Paleozoic reefs and bioherms of West Texas and New Mexico: New Mexico Bureau of Geology and Mineral Resources Open-File Report 504, 166 p.
- Stafford, K. W., R. Nance, L. Rosales-Lagarde, and P. J. Boston, 2008a, Epigene and hypogene karst manifestations of the Castile Formation: Eddy County, New Mexico and Culberson County, Texas. *International Journal of Speleology*, v. 37, p. 83–98.
- Stafford, K. W., L. Rosales-Lagarde, and P. J. Boston, 2008b, Castile evaporite karst potential map of the Gypsum Plain, Eddy County, New Mexico and Culberson County, Texas: A GIS methodological comparison: *Journal of Cave and Karst Studies*, v. 70, p. 35–46.
- Stafford, K. W., D. Ulmer-Scholle, and L. Rosales-Lagarde, 2008c, Hypogene calcitization: Evaporite diagenesis in the western Delaware Basin: *Carbonates and Evaporites*, v. 23, p. 89–103.
- Stafford, K., W. Brown, J. Ehrhart, A. Majzoub, and J. Woodard, 2017, Evaporite karst geohazards in the Delaware Basin, Texas: Review of traditional karst studies coupled with geophysical and remote sensing characterization: *International Journal of Speleology*, v. 46, p. 169–180.
- Stafford, K., J. Ehrhart, A. Majzoub, J. Shields, and W. Brown, 2018, Unconfined hypogene evaporite karst: West Texas and southeastern New Mexico, USA: *International Journal of Speleology*, v. 47, p. 293–305.
- Woodard, J. D., 2017, Geophysical delineation of megaporosity and fluid migration pathways for geohazard characterization within the Delaware Basin, Culberson County, Texas: M.S. Thesis, Stephen F. Austin State University, 137 p.